A DYNAMIC MODEL FOR FLUID FLOW IN A BOREHOLE FRACTURE

by

X.M. Tang, and C.H. Cheng

Earth Resources Laboratory
Department of Earth, Atmospheric, and Planetary Sciences
Massachusetts Institute of Technology
Cambridge, MA 02139

ABSTRACT

The attenuation of Stoneley waves by a borehole fracture are closely related to fluid flow in the fracture. We consider the dynamic response of a viscous fluid in a horizontal fracture to the oscillating pressure excitation of Stoneley waves at the fracture opening. A dynamic model has been developed to describe the fluid motion in the fracture. This model relates both viscous shear effects at the fracture surface and the acoustic wave propagation in the fracture fluid. The dynamic conductivity is derived to characterize the fluid conduction in the fracture. This model is applied to study Stoneley wave attenuation across a borehole fracture, and is found to agree well with laboratory fracture modeling data.

INTRODUCTION

There is an increasing interest in fracture characterization in using both full waveform acoustic logs and VSP surveys. In full waveform logging, a model by Mathieu (1984) has been used to model Stoneley wave attenuation across a fracture. Although qualitative and rough quantitative correlations were found between the model and field data (Hardin et al., 1987), this model is imperfect because it is a kinematic rather than a dynamic model. In VSP surveys, a model by Beydoun et al. (1985) has been used to study tube wave generation by a borehole fracture. In both models, however, fluid flow in the fracture was treated as quasi-static, and the "cubic law" (Snow, 1965) for steady flow was assumed. Since both models deal with dynamic wave phenomena, the validity of this law under dynamic conditions is subject to question. One of the major goals of this study is to investigate the behavior of fluid motions in a fracture under dynamic wave excitations. The results are expected to be an extension of the cubic law into the dynamic regime.

In the first part of this study, dynamic wave equations for a viscous fluid are solved

in conjunction boundary conditions at the fracture surface. This leads to a characteristic equation which governs the relative importance of viscous shear effects and wave propagation effects. On the basis of these solutions and Darcy's law, we derive the dynamic conductivity which characterizes fluid conduction under dynamic conditions. Next, we apply our flow model to study the Stoneley wave attenuation across a borehole fracture and compare the theoretical results with laboratory experimental data. Finally, we discuss the relevance of our model to previous models.

THEORETICAL DEVELOPMENT

In a viscous fluid, a perturbation is governed by the equations of motion and continuity, which are written as

$$\rho\left(\frac{\partial \vec{v}}{\partial t}+\vec{v}\cdot\nabla\vec{v}\right) = -\nabla p+\mu\nabla^2\vec{v}+\frac{\mu}{3}\nabla\nabla\cdot\vec{v} \quad (1)$$

$$\frac{\partial \rho}{\partial t}+\nabla\cdot(\rho\vec{v}) = 0, \quad (2)$$

respectively, where t is time, $\vec{v}$ is the fluid particle velocity, p is the pressure perturbation, abd μ is viscosity. ρ, the density of the fluid, can be written as

$$\rho=\rho_0+\rho', \quad (3)$$

where ρ_0 is the density at equilibrium and ρ' is the density perturbation. Neglecting thermal effects in the fluid, we have the following equation of state for the fluid:

$$p=\alpha_f^2\rho', \quad (4)$$

where α_f is the acoustic velocity of the fluid. Substituting Eqs. (3) and (4) into Eqs. (1) and (2) and using the fact that $\vec{v}$ is also a perturbation, we can linearize Eqs. (1) and (2) by taking only the first order perturbation. In the frequency domain, the linearized equations are:

$$-i\omega\vec{v}+\frac{1}{\rho_0}\nabla p = \nu\nabla^2\vec{v}+\frac{\nu}{3}\nabla\nabla\cdot\vec{v} \quad (5)$$

$$-i\omega p+\rho_0\alpha_f^2\nabla\cdot\vec{v} = 0, \quad (6)$$

where ω is angular frequency and $\nu=\mu/\rho_0$ is the kinematic viscosity. By virtue of vector decomposition, we can write $\vec{v}$ as

$$\vec{v}=\nabla\phi+\nabla\times\vec{\psi}, \quad (7)$$

where ϕ is the acoustic wave potential and $\vec{\psi}$ is the viscous shear potential. Substitution of Eq. (7) into Eqs. (5) and (6) gives

$$\nabla^2\phi+\frac{\omega^2}{\alpha_f^2-\frac{4}{3}i\omega\nu}\phi = 0 \quad (8)$$

$$\nabla^2\vec{\psi} + \frac{i\omega}{\nu}\vec{\psi} = 0 \tag{9}$$

We now apply Eqs. (8) and (9) to study the fluid motion inside a horizontal borehole fracture, which is modeled as a plane-parallel channel of thickness L_0 and of infinite extent. Let us consider cylindrical coordinates (r, φ, z) where r is the distance from the borehole axis, φ is the polar angle, and z is the vertical coordinate, with $z = 0$ at the center of the fracture opening. Assuming axial symmetry of the problem, we can chose $\vec{\psi} = \psi\vec{e}_\varphi$, where $\vec{e}_\varphi$ is the unit vector along the increasing φ direction. Eqs. (8) and (9) may thus be written as

$$\frac{\partial^2\phi}{\partial r^2} + \frac{1}{r}\frac{\partial\phi}{\partial r} + \frac{\partial^2\phi}{\partial z^2} + \frac{\omega^2}{\alpha_f^2 - \frac{4}{3}i\omega\nu}\phi = 0 \tag{10}$$

$$\frac{\partial^2\psi}{\partial r^2} + \frac{1}{r}\frac{\partial\psi}{\partial r} - \frac{\psi}{r^2} + \frac{\partial^2\psi}{\partial z^2} + \frac{i\omega}{\nu}\psi = 0 \ . \tag{11}$$

By separation of variables, solutions of Eqs. (10) and (11) are found to be

$$\phi = H_0^{(1)}(kr)[A\cos(fz) + B\sin(fz)] \tag{12}$$

$$\psi = H_1^{(1)}(kr)[C\cos(\bar{f}z) + D\sin(\bar{f}z)], \tag{13}$$

where:

$$f^2 = \frac{\omega^2}{\alpha_f^2 - \frac{4}{3}i\omega\nu} - k^2 \tag{14}$$

$$\bar{f}^2 = \frac{i\omega}{\nu} - k^2, \tag{15}$$

$H_0^{(1)}$ and $H_1^{(1)}$ are outgoing Hankel functions of order zero and one, $k = \omega/\bar{c}$ is the wavenumber of the fracture fluid, and A, B, C, and D are parameters to be determined.

Characteristic Equation

We now determine the parameters in Eqs. (12) and (13) with the boundary conditions at the fracture surface. Due to the axial symmetry, the fluid particle velocity has only two components. According to Eq. (7), they are

$$\begin{aligned} v_r &= \frac{\partial\phi}{\partial r} - \frac{\partial\psi}{\partial z} \\ &= -H_1^{(1)}(kr)[Ak\cos(fz) + Bk\sin(fz) - C\bar{f}\sin(\bar{f}z) + D\bar{f}\cos(\bar{f}z)] \end{aligned} \tag{16}$$

$$\begin{aligned} v_z &= \frac{\partial\phi}{\partial r} + \frac{\partial\psi}{\partial r} + \frac{\psi}{r} \\ &= H_0^{(1)}(kr)[-Af\sin(fz) + Bf\cos(fz) + Ck\cos(\bar{f}z) + Dk\sin(\bar{f}z)] \end{aligned} \tag{17}$$

We assume that the formation is rigid. This is appropriate when the fracture is in a hard formation whose elastic moduli and density are much larger than those of the fluid. Thus the viscous non-slip boundary condition at the fracture surface gives

$$v_r = v_z = 0, \quad (at\ z = \pm\frac{L_0}{2}) \tag{18}$$

Substitution of Eqs. (16) and (17) into Eqs. (18) results in a system of homogeneous equations:

$$\mathbf{Gx} = 0 \tag{19}$$

where:

$$\mathbf{x}^T = [A\ B\ C\ D] \quad , \tag{20}$$

and $\mathbf{G}$ is a 4 × 4 matrix whose elements are given by the terms such as $k\cos(f\frac{L_0}{2})$, $\bar{f}\sin(\bar{f}\frac{L_0}{2})$, etc. (Eqs. 16 and 17). For $\mathbf{x}$ to have a non-trivial solution, the determinant of $\mathbf{G}$ must vanish and this leads to the following characteristic equation:

$$k^2\tan(\bar{f}\frac{L_0}{2}) + f\bar{f}\tan(f\frac{L_0}{2}) = 0 \tag{21}$$

The above is an important equation because it relates both viscous shear and acoustic propagation effects in the fracture. As a result, $k = \omega/\bar{c}$ is no longer the free space wavenumber, wave dispersion and attenuation will both occur. When k is found by solving this complex equation, the velocity dispersion is determined and the quality factor of the fracture fluid is given by

$$Q_f = \frac{Re\{k\}}{Im\{k\}} \quad . \tag{22}$$

Figure 1 plots the wave velocity and Q_f versus frequency for different fracture widths. The fluid is water ($\rho = 1\ g/cm^3$, $\mu = 0.01gs^{-1}cm$, and $\alpha_f = 1500m/sec$). As seen from this figure, the velocity and Q_f are substantially reduced with decreasing aperture and frequency. This can be understood because viscous shear is mostly a boundary layer effect (Burns, 1988).

Dynamic Conductivity of Fracture Fluid

It is well known that fluid conduction in a fracture under a static pressure gradient obeys the cubic law (Snow, 1965). The fluid conduction in a fracture under dynamic pressure excitations is of particular interest of this section. By using k determined from Eq. (21), a non-trivial solution of $\mathbf{x}$ in Eq. (20) can be found, whose elements are specificly given as

$$\begin{aligned} B &= 0 \\ C &= 0 \\ D &= -\frac{k\cos(f\frac{L_0}{2})}{\bar{f}\cos(\bar{f}\frac{L_0}{2})}A \quad . \end{aligned} \tag{23}$$

Therefore, only one parameter (say A) needs to be found, and it is determined by pressure continuity at the fracture opening. By using Eqs. (6), (7), and (12), pressure in the fracture is found to be

$$p = \frac{i\omega\rho_0 A}{1 - \frac{4i\omega\nu}{3\alpha_f^2}} H_0^{(1)}(kr)\cos(fz) \quad . \tag{24}$$

At the fracture opening $r = R$, Eq. (24) is averaged over the fracture width L_0 to match the borehole fluid pressure $p(\omega, R)$, which is taken to be independent of z because L_0 is small compared with the Stoneley wave wavelength (Hardin et al., 1987). By so doing, A is determined as

$$A = \frac{p(\omega, R)(1 - \frac{4i\omega\nu}{3\alpha_f^2})\frac{fL_0}{2}}{i\omega\rho_0 H_0^{(1)}(kR)\sin(\frac{fL_0}{2})} \quad . \tag{25}$$

Once A is known, the fluid motion in the fracture is completely specified by Eqs. (16) and (17). We can therefore find the fluid flow conducted into the fracture opening, which is given by

$$\begin{aligned} q^{(F)} &= 2\pi R \int_{-\frac{L_0}{2}}^{\frac{L_0}{2}} v_r dz, \quad (at\ r = R) \\ &= -\frac{i\omega L_0}{k^2\alpha_f^2\rho_0}\left[-p(\omega, R)k\frac{H_1^{(1)}(kR)}{H_0^{(1)}(kR)}\right] 2\pi R \quad . \end{aligned} \tag{26}$$

By differentiating Eq. (24) with respect to r and using Eq. (25), it is readily shown that the term in square brackets in Eq. (26) is the pressure gradient $\partial p/\partial r$ averaged over L_0 and evaluated at the borehole radius $r = R$. Comparing Eq. (26) with Darcy's law

$$q = -\bar{C}|\nabla p|, \tag{27}$$

where q is the flow rate per unit length (analogous to $q^{(F)}/2\pi R$ in Eq. 26) and $\bar{C}$ is the hydraulic conductivity for the steady state case, we see that the term in front of the square brackets in Eq. (26) is analogous to $\bar{C}$, and is hereby defined as the dynamic conductivity of the fracture:

$$\bar{C} \equiv \frac{i\omega L_0}{k^2\alpha_f^2\rho_0} \quad , \tag{28}$$

where k is given by the solution to Eq. (21). It should be emphasized that, although Eqs. (21) and (28) are obtained with a borehole geometry, they are also valid in general fracture fluid flow problems. The asymptotic behaviors of $\bar{C}$ at low and high frequencies (or small and large flow apertures) can be readily obtained. By letting $\omega \rightarrow 0$ and

$\omega \rightarrow \infty$ respectively, Eq. (21) can be solved asymptotically to give (See Appendix)

$$k^2 = \frac{12i\omega\nu}{\alpha_f^2 L_0^2}, \quad (\omega \rightarrow 0) \tag{29}$$

$$k^2 = \frac{\omega^2}{\alpha_f^2}, \quad (\omega \rightarrow \infty) \tag{30}$$

where we have neglected the free space attenuation term $\frac{4i\omega\nu}{3\alpha_f^2}$, because it is small compared to unity. Eq. (29) agrees with Rayleigh's (1945) result for sound propagation in an exceedingly narrow aperture. Substituting Eqs. (29) and (30) into Eq. (28), we have

$$\bar{C} = \frac{L_0^3}{12\mu}, \quad (\omega \rightarrow 0) \tag{31}$$

$$\bar{C} = \frac{iL_0}{\omega\rho_0}, \quad (\omega \rightarrow \infty) \tag{32}$$

Eq. (31) is exactly the cubic law. Thus our definition is consistent with this well defined law at low frequencies. Whereas at high frequencies, $\bar{C}$ becomes a purely imaginary quantity, decreasing with frequency as ω^{-1}. This means that the fluid conduction will be largely reduced as $\omega \rightarrow \infty$. Figure 2 plots the amplitude and phase of the dynamic conductivity for different flow apertures. The amplitudes reach the highest value given by the cubic law at the zero frequency, and decreases with increasing frequency. The larger the aperture, the faster they decrease, as indicated in Figure 2a. Figure 2b is a complement to Figure 2a showing the phase of $\bar{C}$ approaches $\pi/2$ as frequency increases. The larger the aperture, the faster the phase approaches this value, at which $\bar{C}$ becomes an imaginary quantity.

APPLICATION TO STONELEY WAVE ATTENUATION ACROSS A FRACTURE

In this section, we apply the fracture fluid flow model to study Stoneley wave attenuation across a single borehole fracture. Using the same cylindrical coordinates described previously, the borehole fluid pressure due to Stoneley waves can be written as (Biot, 1952)

$$p^{(l)} = E^{(l)} I_0(nr) e^{\pm i\kappa z} \quad , \tag{33}$$

where I_0 is the zeroth order modified Bessel function of the first kind and $E^{(l)}$'s are as yet undetermined coefficients. Eq. (33) includes Stoneley waves incident on ($l = I$, $e^{\pm i\kappa z} \rightarrow e^{+i\kappa z}$), reflected back from ($l = R$, $e^{\pm i\kappa z} \rightarrow e^{-i\kappa z}$), and transmitted across ($l = T$, $e^{\pm i\kappa z} \rightarrow e^{+i\kappa z}$) the fracture opening, and

$$n^2 = \kappa^2 (1 - \frac{c^2}{\alpha_f^2}) \quad , \tag{34}$$

where $\kappa = \omega/c$ and c is the Stoneley wave phase velocity. The axial particle velocity in the borehole fluid is given by

$$v_z^{(l)} = \frac{1}{i\omega\rho_0}\frac{\partial p^{(l)}}{\partial z}, \quad (l = I, R, T). \tag{35}$$

Since fracture width L_0 is generally small, no substantial pressure drop will occur across the fracture. Pressure continuity gives

$$p^{(I)} + p^{(R)} = p^{(T)}, \quad (at\ z = 0) \tag{36}$$

Substituting Eq. (33) into Eq. (36), we obtain

$$E^{(T)} = E^{(I)} + E^{(R)} \tag{37}$$

Under dynamic conditions, volume conservation of fluid flow is governed by Eq (6). Integrating this equation over a small volume ΔV and applying the divergence theorem, we obtain

$$-\oint_S \vec{v}\cdot d\vec{S} = \frac{i\omega}{\rho_0\alpha_f^2}\int_{\Delta V} -p dV \quad , \tag{38}$$

where $\Delta V = \pi R^2 L_0$ is a flat cylinder of height L_0 and radius R located at the fracture opening, and S is the surface enclosing ΔV. The normal to S is pointed outwards from ΔV. Eq. (38) has the simple physical meaning that the net flow into ΔV equals the dynamic volume compression of ΔV. In previous models of Mathieu (1984) and Hornby et al. (1988), this dynamic effect was not taken into account. However, as will be shown later, this effect is generally not very significant. The net flow into ΔV is

$$-\oint_S \vec{v}\cdot d\vec{S} = q^{(I)} + q^{(R)} - q^{(T)} - q^{(F)} \quad (at\ z \approx 0) \quad , \tag{39}$$

where

$$q^{(l)} = 2\pi\int_0^R v_z^{(l)} r dr, \quad (l = I, R, T), \tag{40}$$

and $q^{(F)}$ is the flow away from ΔV into the fracture, as given by Eq. (26). If we approximate the pressure inside ΔV by the transmitted pressure $p^{(T)}$, the volume integral in Eq. (38) is given by

$$\int_{\Delta V} p^{(T)} dV = 2\pi L_0 \frac{R}{n} I_1(nR) E^{(T)} \quad , \tag{41}$$

where I_1 is the first order modified Bessel function of the first kind. When the integration in Eq. (40) is completed using Eqs. (33) and (35), Eqs. (38) and (41) are combined to give

$$q^{(F)} = \frac{2\pi R}{\rho_0 c n} I_1(nR)\left[E^{(I)} - E^{(R)} - (1 - \frac{i\omega c L_0}{\alpha_f^2})E^{(T)}\right] \tag{42}$$

Equating the pressure at the fracture opening (i.e., $p(w,R)$ in Eq. 26) to $p^{(T)}(\omega,R)$, we have

$$p(\omega,R) = E^{(T)} I_0(nR) \quad . \tag{43}$$

Eqs. (38) and (42), together with Eqs. (26) and (43), are solved to give the reflection and transmission coefficients of the waves. They are:

$$R_{ef} = \frac{E^{(R)}}{E^{(I)}} = -\frac{Y}{1+Y} \tag{44}$$

$$T_{rs} = \frac{E^{(T)}}{E^{(I)}} = \frac{1}{1+Y} \tag{45}$$

where:

$$Y = \frac{\rho_0 c}{2}\bar{C}\left[kn\frac{I_0(nR)}{I_1(nR)}\frac{H_1^{(1)}(kR)}{H_0^{(1)}(kR)} - k^2\right] \quad , \tag{46}$$

where $\bar{C}$ is the dynamic conductivity given by Eq. (28). Thus we see that when a Stoneley wave comes across a borehole fracture, part of the wave is reflected at the fracture opening, resulting in the attenuation of the wave amplitude of the transmitted wave. Figure 3 shows the amplitude of the transmission coefficent $|T_{rs}|$ as the function of fracture width L_0 for different frequencies. We use a borehole diameter of $7.62cm$. The borehole fluid is water ($\alpha_f = 1500m/s$), and the Stoneley wave velocity is taken to be $0.95\alpha_f$. The general behavior of $|T_{rs}|$ decreases with L_0 and increases with frequency.

Comparison Between Theory and Laboratory Experiment

Eqs. (44), (45), and (46) quantify the wave amplitude partition at the fracture opening. It is desirable to test the theoretical results with a laboratory fracture modeling experiment. Such an experiment was conducted by Poeter (1987). In this experiment, the borehole radius was scaled to $0.3175cm$, the borehole fluid was tap water, and the formation was constructed of concrete. Frequency of the Stoneley wave varied from 40 to 130 kHz. The transmitted Stoneley wave frequencies were centered around 70 kHz. The measured transmitted wave amplitude of the fractured formation was compared with that of the unfractured case and of the "closed" fracture case, respectively. In the former case, the reduction in the wave amplitude was substantial, probably due to the effect of formation discontinuity regardless of aperture. In the latter case, this effect is a common effect on both "closed" and "open" fracture and can be removed by taking the ratio of the latter data relative to the former data. As a result, comparison of the fractured data with the "closed" fracture data mainly reflects the effect of fluid flow into the fracture. The data from Poeter's (1987) Figure 6 for $5.1cm$ source-receiver spacing across a horizontal fracture are used. Figure 4 plots the amplitude of the theoretical transmission coefficient given by Eq. (45) versus the experimental

data. The theoretical curves are calculated for $\omega = 2\pi \times 70$ kHz, $R = 0.3175cm$, and $\alpha_f = 1500m/s$. For calculating n in Eq. (45) given by Eq. (34), we use $c = 1340m/s$, the measured Stoneley wave velocity. The dashed curve in this figure is calculated without the dynamic volume compression term in Eq. (38), while the solid courve is calculated with this term. The correction is minor. As seen from this figure, the theory well fits the data with the $5.1cm$ source-receiver spacing (solid triangles). The open triangles are the data averaged for different source-receiver spacings ranging from 5.1–$22.9cm$ (see Poeter, 1987, Figure 8). The two sets of data give a rough quantitative measure of the accuracy and repeatability of the measurements. Although there is a systematic difference between the average data and the theory, they show the same general decreasing tendency with increasing fracture width. Considering errors in the experimental data, we can say that the theory fits the data reasonably well.

DISCUSSION

In this study, the fluid motion inside a fracture with rigid walls is vigorously solved by relating both viscous shear effect and acoustic propagation effect. The relative importance of these two effects is governed by a complex equation (Eq. 21). When the former effect dominates, the fluid motion is diffusive, while when latter effect dominates, the motion is propagational. A qualitative criterion is the viscous "skin depth" $\delta = \sqrt{2\nu/\omega}$. For example, taking $\omega = 2\pi \times 1000$ Hz, the skin depths for water and mud ($\mu_{mud} \approx 100\mu_{water}$, Burns, 1988) are about $20\mu m$ and $200\mu m$, respectively. We have seen in Figure 1 that when, $L_0 > 100\mu m$, the velocity dispersion is not very significant (the fluid is water.). Also, as we have seen in Figure 2, the dynamic conductivity for the small aperture ($L_0 = 10\mu m$) curve is nearly constant (the cubic law). The conductivity decreases with increasing frequency when the flow aperture is large. These examples demonstrate that, for fractures with large apertures, fluid flow is mainly a propagational effect. However, when the flow aperture is the order of 2δ, viscous effects will control the fluid motion.

We now discuss the relevance of our model to previous models of Mathieu (1984) and Hornby et al. (1987). In Mathieu's model, flow in the fracture was assumed diffusive and the fracture conductivity was given by the cubic law. In addition, pressure excitation at the borehole opening was treated as quasi-static by averaging it over the half cycle. An important parameter of this model is the fluid diffusivity in the diffusion equation (Mathieu, 1984)

$$b = \frac{L_0^2}{12\gamma\mu}$$

where $\gamma = \rho^{-1}(\frac{\partial\rho}{\partial p})_T$ is the fluid compressibility. We can show that $i\omega/b$ is our k^2 in

Eq. (29) at low frequencies. Using the thermodynamic relation,

$$(\frac{\partial \rho}{\partial p})_T = \frac{C_p}{C_v}(\frac{\partial \rho}{\partial p})_S,$$

where S denotes entropy while T temperature. For fluid, the ratio of the heat capacities $C_p/C_v \approx 1$. Thus $\gamma \approx \rho^{-1}(\frac{\partial \rho}{\partial p})_S = \rho^{-1}\alpha_f^{-2}$. This immediately gives

$$\frac{i\omega}{b} = \frac{12i\omega\nu}{\alpha_f^2 L_0^2},$$

agreeing with Eq. (29), where $k^2 \propto i\omega$ implies that the wave motion is diffusive. Thus our model reduces to Mathieu's model at low frequencies or small apertures. However, Mathieu (1984) modeled the pressure excitation as a step function in the time domain, which is inconsistent with our dynamic model. In addition, Mathieu's model predicts that the transmission coefficient is minimally dependent on frequency, whereas ours can be strongly dependent on frequency. This implies that when using the present model to determine flow aperture, this frequency dependency has to be taken into account. Moreover, in order to produce a specific attenuation, the present model generally requires a larger flow aperture than Mathieu's model does.

In the Hornby et al. (1987) model, the fluid motion in a fracture is purely propagational. This is valid when the fracture fluid has very low viscosity (such as water), the fracture aperture is not very small, and the frequency is high. In fact, under the above mentioned conditions, the fracture fluid wavenumber, as determined by Eq. (21), approaches the free space wavenumber, and the fluid motion becomes propagational. Therefore, under these conditions, the present model is almost identical to the Hornby et al. model. However, as shown in the previous section, at 1 kHz, the viscous skin depth is of the order of 20 to 200 microns, depending on the viscosity. In situ fracture apertures of the order of 100 microns are not uncommon. In VSP's, lower frequency means that the skip depth is even greater, of the order of 500 microns or more, and thus we must take the viscous effect into account for this to be a complete theory. The present model is a complete theory valid for any flow aperture, fluid viscosity, and frequencies.

CONCLUSIONS

The major results of this study can be summarized as follows:

- Fluid motion in a narrow aperture has been treated by considering both viscous shear and wave propagation effects. A characteristic equation has been obtained (Eq. 21), which governs the relative importance of the two effects. The viscous

effect resists fluid flow and is important for very narrow apertures or high viscosity fluids, especially at low frequencies. Outside of these situations, fluid motion is mostly propagational.

- Under dynamic pressure excitations, fluid conduction in a fracture is characterized by the dynamic conductivity (Eq. 28), which reduces to the cubic law at low frequencies or small flow apertures. This dynamic flow law, instead of the cubic law, can be applied to dynamic flow problems in a fracture. An immediate application of this is to use the dynamic conductivity in place of cubic law conductivity in the tube wave generation model (Beydoun et al., 1985) in VSP surveys.

- The present flow model has been used to study Stoneley wave attenuation across a borehole fracture and the theoretical results are found to agree well with laboratory fracture modeling data.

ACKNOWLEDGEMENTS

This research was supported by Department of Energy grant No. DE-FG02-86ER13636, and by the Full Waveform Acoustic Logging Consortium at M.I.T.

REFERENCES

Beydoun, W.B., Cheng, C.H., and Toksöz, M.N., Detection of open fractures with vertical seismic profiling, *J. Geophys. Res., 90,* 4557–4566, 1985.

Biot, M.A., Propagation of elastic waves in a cylindrical bore containing a fluid, *J. Appl. Phys., 23,* 977–1005, 1952.

Burns, D.R., Viscous fluid effects on guided wave propagation in a borehole, *J. Acoust. Soc. Am., 83,* 463–469, 1988.

Cheng, C.H. and Toksöz, M.N., Elastic wave propagation in a fluid-filled borehole and synthetic acoustic logs, *Geophysics, 46,* 1042–1053, 1981.

Hardin, E.L., Cheng, C.H., Paillet, F.L., and Mendelson, J.D., Fracture characterization by means of attenuation and generation of tube waves in fractured crystalline rock at Mirror Lake, New Hampshire, *J. Geophys. Res., 92,* 7989–8006, 1987.

Hornby, B.E., Johnson, D.L., Winkler, K.W., and Plumb, R.A., Fracture evaluation from the borehole Stoneley wave, *Expd. Abst., Soc. Expl. Geophys. 57th Ann. Int. Mtg. and Exposition,* New Orleans, Louisiana, 1987.

Mathieu, F., Application of full waveform acoustic logging data to the estimation of reservior permeability, S.M. thesis, M.I.T., Cambridge, 1984.

Poeter, E.P., Characterizing fractures at potential nuclear waste repository sites with acoustic waveform logs, *The Log Analyst, 28,* 453–461, 1987.

Rayleigh, J.B., *The Theory of Sound,* Dover Publications, 327–328, 1945.

Snow, D.T., A parallel plate model of fractured permeability media, Ph.D. thesis, Univ. of Calif., Berkeley, 1965.

APPENDIX

Low and High Frequency Behaviors of Eq. (21)

In this appendix, we find asymptotic behaviors of Eq. (21) at low and high frequencies. When the argument of the tangent function is small (this condition can be satisfied by requiring either low frequencies or small flow apertures), the tangent functions in Eq. (21) can be expanded in a Taylor series

$$\tan(f\frac{L_0}{2}) \sim f\frac{L_0}{2} + \frac{1}{3}(f\frac{L_0}{2})^3 + \cdots \quad \text{(A-1)}$$

$$\tan(\bar{f}\frac{L_0}{2}) \sim \bar{f}\frac{L_0}{2} + \frac{1}{3}(\bar{f}\frac{L_0}{2})^3 + \cdots \quad \text{(A-2)}$$

Substitution of the above equations into Eq. (21) results in

$$k^2 + f^2 + \frac{L_0^2}{12}\bar{f}^2k^2 + \frac{L_0^2}{12}f^4 \approx 0 \quad (A-3)$$

Solving this equation, we find

$$k^2 = \frac{\dfrac{\omega^2}{\alpha_f^2 - \frac{4}{3}i\omega\nu} + \dfrac{12}{L_0^2}}{2 + \dfrac{\alpha_f^2 - \frac{4}{3}i\omega\nu}{i\omega\nu}} \quad (A-4)$$

The second term in both numerator and denominator of above equation is much larger than the first term. This results in

$$k^2 \approx \frac{12i\omega\nu}{L_0^2\alpha_f^2(1 - \frac{4i\omega\nu}{3\alpha_f^2})} \quad (A-5)$$

When the frequency is high, we can rewrite Eq. (21) as

$$\frac{f\bar{f}}{k^2} = -\frac{\tan(\bar{f}\frac{L_0}{2})}{\tan(f\frac{L_0}{2})} \quad (A-6)$$

As the argument of the tangents $\to \infty$ (this condition requires that either ω or L_0 be large), $\tan(\bar{f}\frac{L_0}{2}) \to i$ and $\tan(f\frac{L_0}{2}) \to i$. The RHS of the above equation approaches -1. This gives

$$k^2 + \sqrt{\frac{i\omega}{\nu} - k^2}\sqrt{\frac{\omega^2}{\alpha_f^2 - \frac{4}{3}i\omega\nu} - k^2} \approx 0 \quad (A-7)$$

The solution of this equation is

$$k^2 = \frac{\frac{i\omega}{\nu}\frac{\omega^2}{\alpha_f^2 - \frac{4}{3}i\omega\nu}}{\frac{i\omega}{\nu} + \frac{\omega^2}{\alpha_f^2 - \frac{4}{3}i\omega\nu}} \qquad (A-8)$$

The first term in the denominator is much larger than the second term, even at high frequencies. Thus we obtain

$$k^2 \approx \frac{\omega^2}{\alpha_f^2(1 - \frac{4i\omega\nu}{3\alpha_f^2})} \qquad (A-9)$$

The free space attenuation term $\frac{4i\omega\nu}{3\alpha_f^2}$ is very small compared to unity, and can be neglected.

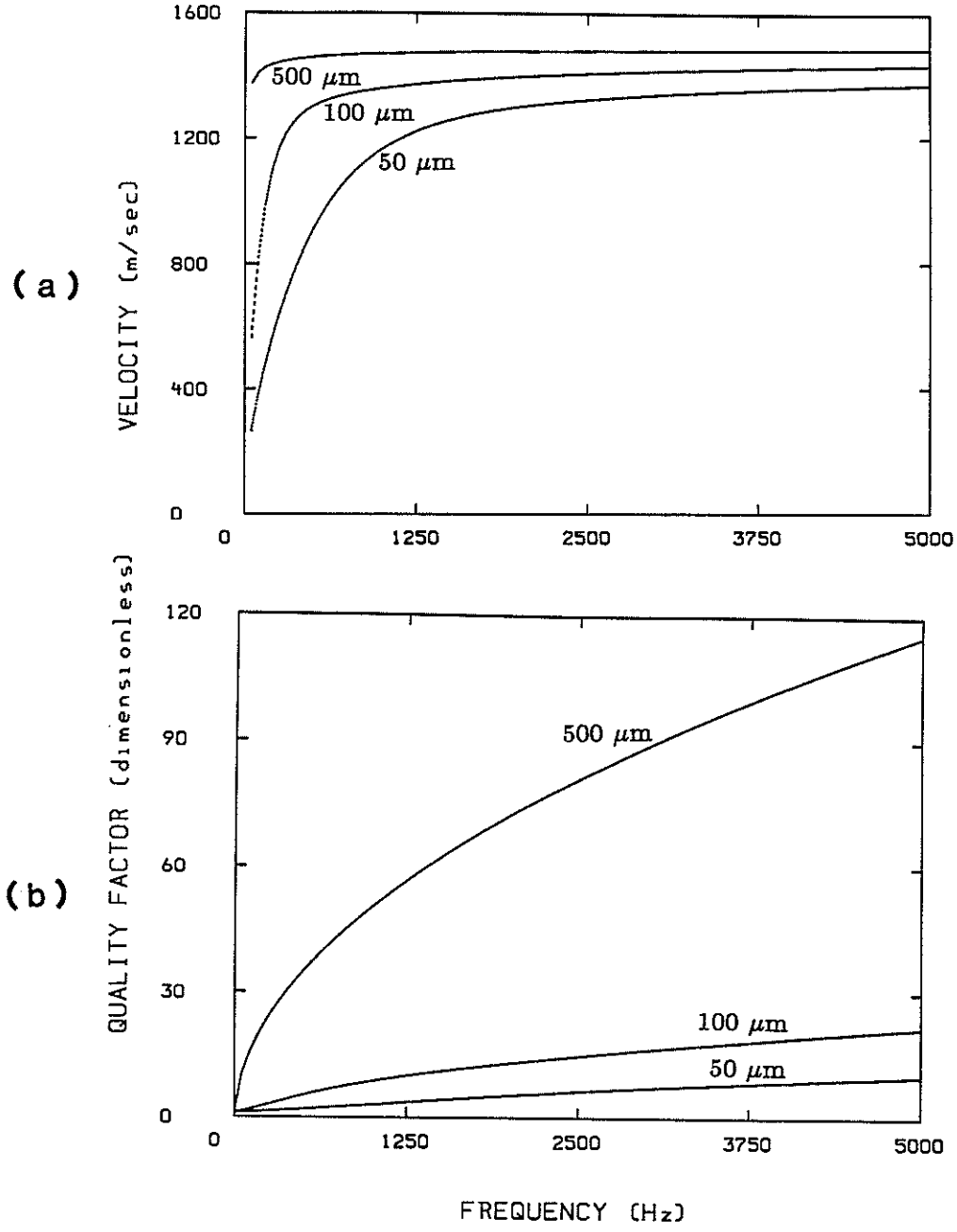

Figure 1: Velocity dispersion and attenuation of wave motion in a fracture. (a) Velocity versus frequency for fracture widths of 50, 100, and 500 microns. The fracture fluid is water. (b) Quality factor for the fracture fluid. The parameters are the same as in (a).

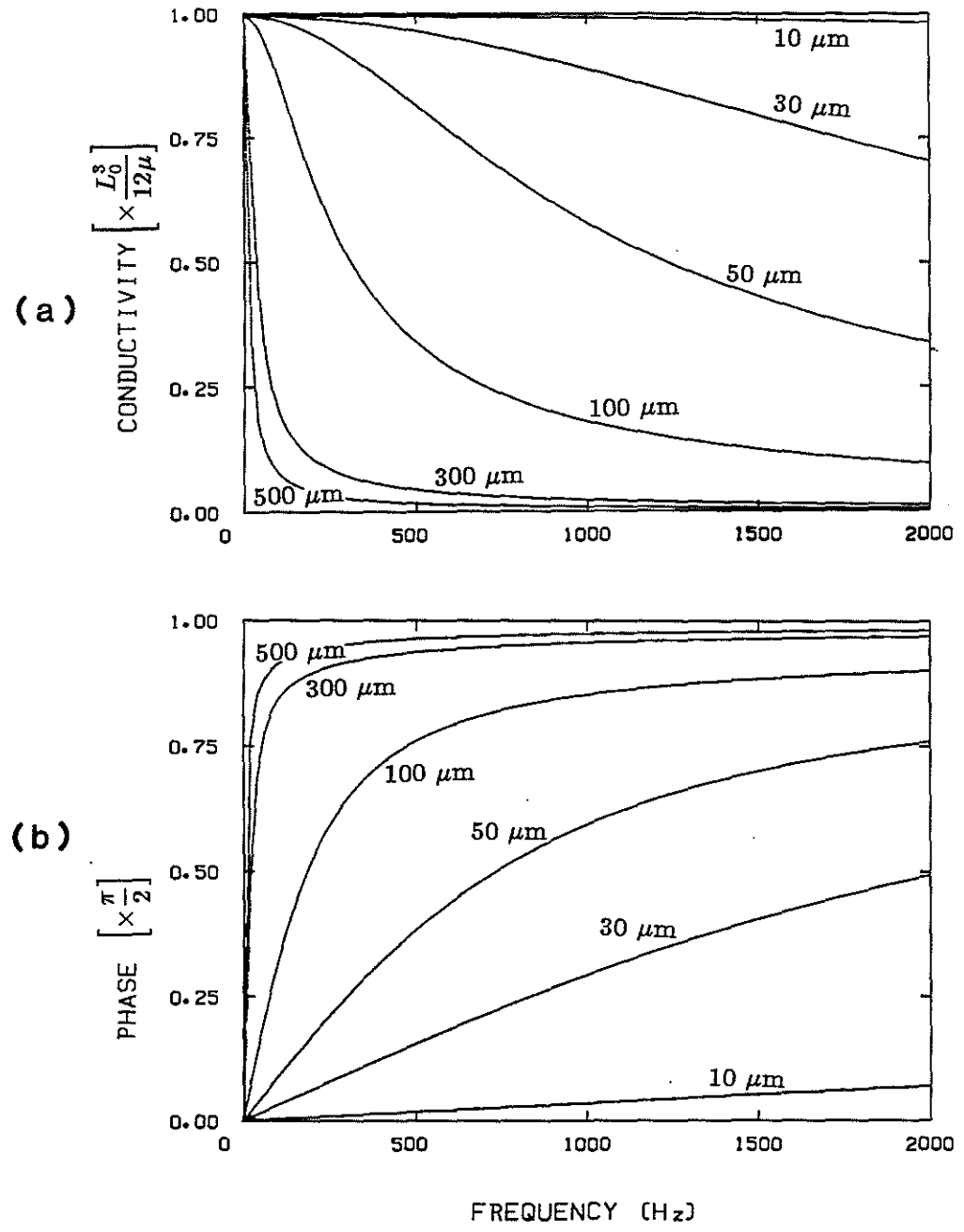

Figure 2: (a) Amplitude of the dynamic conductivity versus frequency for different fracture widths. The amplitudes are normalized by their zero frequency value $L_0^3/12\mu$ (the cubic law). (b) Phase of the dynamic conductivity versus frequency for different fracture widths.

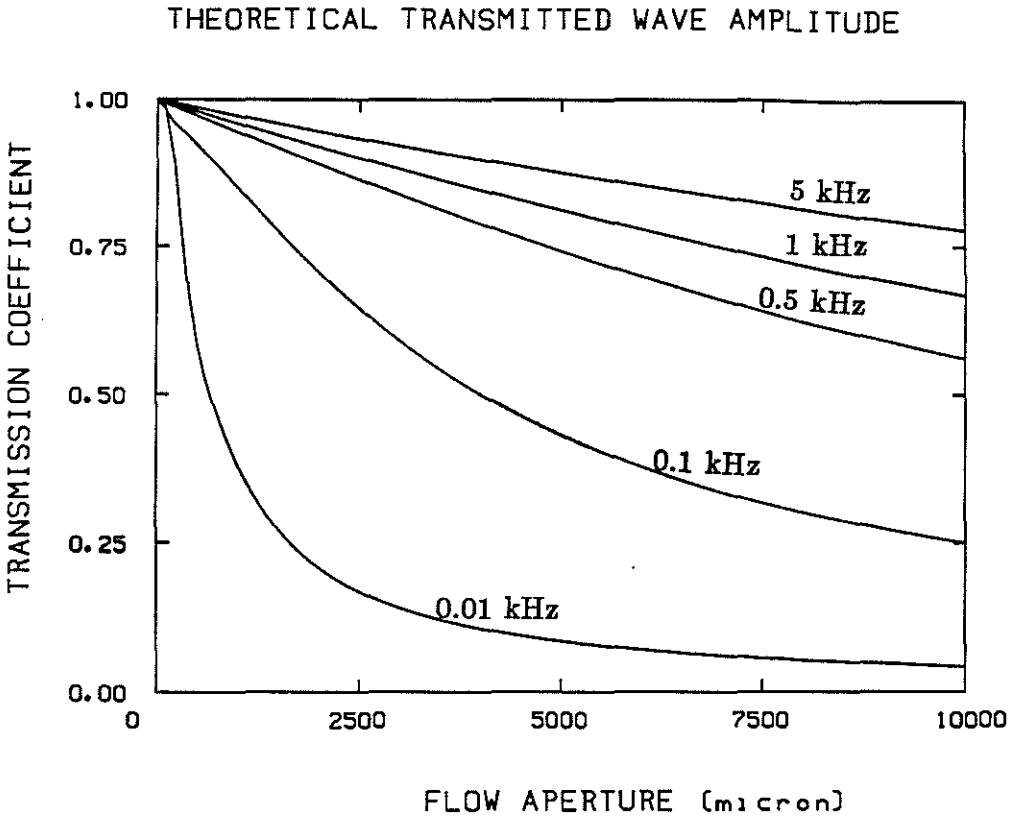

Figure 3: Amplitude of the theoretical transmission coefficient versus fracture width for different frequencies. The parameters are: $R = 3.81cm$, $\alpha = 1500m/s$, and $c = 0.95\alpha_f$.

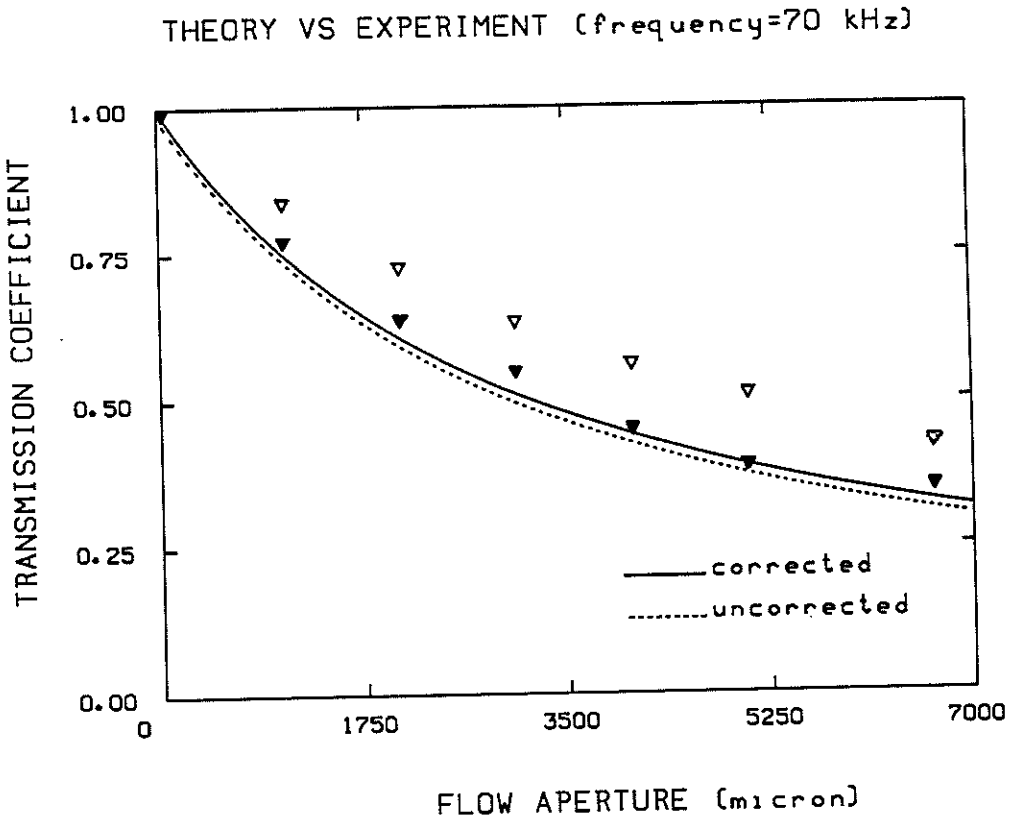

Figure 4: Comparison of theory with laboratory experimental data. The parameters are: $R = 0.3175cm$, $\alpha_f = 1500m/s$, $c = 1340m/s$, and $\omega = 2\pi \times 70$ kHz. The dashed curve is calculated without the dynamic compression term in Eq. (38). The solid curve is corrected for this effect. The theory fits the data with the $5.1cm$ source-receiver spacing (solid triangles). The open triangles are the data averaged for four different source-receiver spacings ranging from 5.1–22.9cm.